Mon. Not. R. Astron. Soc. **000**, 1–13 (0000) Printed 28 February 2011 (MN LATEX style file v2.2)

Evidence for a circum-nuclear and ionised absorber in the X-ray obscured Broad Line Radio Galaxy 3C 445

V. Braito[1]*; J.N. Reeves[2]; R.M. Sambruna[3]†, J. Gofford[2]
[1]*X-Ray Astronomy Observational Group, Department of Physics and Astronomy, Leicester University, Leicester LE1 7RH, UK*
[2]*Astrophysics Group, School of Physical and Geographical Sciences, Keele University, Keele, Staffordshire ST5 5BG*
[3]*Astrophysics Science Division, Mail Code 662, NASA Goddard Space Flight Center, Greenbelt, MD 20771, USA*

ABSTRACT

Here we present the results of a *Suzaku* observation of the Broad Line Radio Galaxy 3C 445. We confirm the results obtained with the previous X-ray observations which unveiled the presence of several soft X-ray emission lines and an overall X-ray emission which strongly resembles a typical Seyfert 2 despite of the optical classification as an unobscured AGN.
The broad band spectrum allowed us to measure for the first time the amount of reflection ($R \sim 0.9$) which together with the relatively strong neutral Fe Kα emission line ($EW \sim 100$ eV) strongly supports a scenario where a Compton-thick mirror is present. The primary X-ray continuum is strongly obscured by an absorber with a column density of $N_{\rm H} = 2 - 3 \times 10^{23}{\rm cm}^{-2}$. Two possible scenarios are proposed for the absorber: a neutral partial covering or a mildly ionised absorber with an ionisation parameter $log\xi \sim 1.0$ erg cm s^{-1}. A comparison with the past and more recent X-ray observations of 3C 445 performed with XMM-*Newton* and *Chandra* is presented, which provided tentative evidence that the ionised and outflowing absorber varied. We argue that the absorber is probably associated with an equatorial disk-wind located within the parsec scale molecular torus.

Key words: galaxies: active – galaxies: individual (3C 445) – X-rays: galaxies

1 INTRODUCTION

X-ray observations of AGN are a powerful tool to understand the physical conditions of the matter in the proximity of the central SMBH and to understand the possible connection between the accretion and outflow mechanisms. In the last decade X-ray observations have confirmed the widely accepted Unified Model (Antonucci 1993) of AGN, which accounts for the difference between type 1 and type 2 AGNs through orientation effects. However there are still several open questions related to the geometry, and physical state of the matter in the proximity of the central supermassive black hole (SMBH). In particular a key question still to be answered is the origin of powerful relativistic jets and outflowing winds. Understanding the nature of AGN with powerful jets or disk winds is not only important in order to understand the accretion itself, but more importantly the mechanism with which the AGN can expel the gas supply of the host galaxy quenching the growth of the SMBH and of the galaxy itself. Indeed, jets and outflows can transport a significant fraction of the mass-energy into the AGN environment and they could represent a key to understand the AGN feedback mechanism (Fabian 2010; Elvis 2006; Cattaneo et al. 2009; King & Pounds 2003).

In the last decade X-ray observations have successfully revealed the presence of both warm and cold gas in the central region of AGN, and have shown that $\sim$ 50% of the X-ray spectra of radio quiet AGN (RQ-AGN) present absorption and emission features due to the presence of photoionised gas, which is outflowing with typical velocities of $\sim 100 - 1000$ km s^{-1} (Crenshaw et al. 2003). On the other end, previous observations of Radio-Loud AGN (RL-AGN) suggested that their X-ray emission is similar to the case of RQ AGN but with some differences. In particular the X-ray emission appears to be harder (or flatter) and with weaker features due to reprocessing (reflection/absorption) from warm or cold gas with respect to the RQ population (Sambruna et al. 2002; Grandi et al. 2006; Ballantyne 2007). Several possible scenarios were proposed to account for these differences, among them a smaller subtending angle of the reprocessing medium as in an advection dominated accretion-flow (ADAF) models (Narayan & Yi 1995) or a higher ionisation state of the accretion disk (Ballantyne et al. 2002).

Recent sensitive and broadband observations performed with

continuum shapes where the RL sources simply populate one end of the distribution. Emission and absorption lines have been now detected also in the soft X-ray spectra of Radio Galaxies (Torresi et al. 2010; Reeves et al. 2010, 2009; Torresi et al. 2009; Sambruna et al. 2007; hereafter S07), indicating the presence of photoionised gas in the central regions of RL-AGN analogous to RQ-AGN. Furthermore a recent analysis of the *Suzaku* observations of broad line radio galaxies (BLRGs) has also unveiled the presence of fast outflowing gas with velocities $v \sim 0.1 - 0.3c$ and carrying substantial masses and kinetic powers similar to the radio jets (Tombesi et al. 2010).

We are currently carrying out a program of *Suzaku* observations of a sample of all the nearby ($z < 0.1$) broad line radio galaxies (BLRGs), for which we also have XMM-*Newton* and or *Chandra* data (3C 390.3; Sambruna et al. 2009, 3C 111; Ballo et al. in prep; 3C 382; Sambruna et al. in prep and 3C 445; Reeves et al. 2010). One of the goals of this project is to investigate the structure of the accretion flow and the presence of warm and cold gas in the central regions of BLRGs to better understand the jet formation. Here we focus on one of these sources 3C 445, while the X-ray properties of the sample will be presented in a forthcoming paper (Sambruna et al. in prep).

1.1 The Broad Line Radio Galaxy 3C 445.

3C 445 is a nearby (z=0.057) BLRG with a FRII morphology (Kronberg et al. 1986). The optical spectrum of 3C 445 shows the presence, in total flux, of broad emission lines (Hα FWHM ~6400 km s^{-1}; Eracleous & Halpern 1994) typical of a type 1 or unobscured AGN leading to the classification as a BLRG. The optical continuum is also highly reddened; from the large Balmer decrement (Hα/Hβ $\sim$ 8) Crenshaw et al. 1988 derived E(B-V)=1 mag, consistent with the large Paα/Hβ ratio (5.6; Rudy & Tokunaga 1982). Assuming a standard dust-to-gas ratio this corresponds to a column density of $N_H \sim 5 \times 10^{21}$ cm^{-2}, which is one order of magnitude larger than the Galactic column density in the direction to 3C 445 ($N_H^{Gal} = 5.33 \times 10^{20}$ cm^{-2}, Murphy et al. 1996). From radio observations (Eracleous & Halpern 1998) an inclination for the jet of $i > 60°$ is inferred, suggesting that the contribution of the jet is negligible (Doppler factor of $\delta \sim 0.2$) and also that 3C 445 is seen almost edge-on. A large viewing inclination angle for 3C 445 ($i \leqslant 60°$) was also inferred by Grandi et al. (2007) with the analysis of the flux ratio of the jet components and the VLA maps presented by Leahy et al. (1997).

3C 445 is a bright X-ray source ($F_{2-10\ keV} \sim 7 \times 10^{-12}$ erg cm^{-2} s^{-1}), and was previously observed with all the major X-ray observatories. The analysis of an archival 15 ks XMM-*Newton* observation of 3C 445 showed a remarkable spectrum (S07; Grandi et al. 2007). The intriguing result was that, despite its optical classification as a type 1 AGN, its X-ray emission was typical of an obscured AGN in several aspects. The 2–10 keV continuum could be described by a heavily absorbed ($N_H \sim 10^{23}$ cm^{-2}) power-law with photon index $\Gamma \sim 1.4$; a narrow and unresolved Fe Kα emission line was also detected with EW $\sim$ 120 eV. Due to the limited EPIC bandpass (0.4–10 keV) it was impossible to distinguish between a scenario with a strong reflection component (with $R \sim 2$) or a multi-layer neutral partial covering absorber. Seyfert 2, with several emission lines in 0.6–3 keV, due to ionised elements from O to Si.

At high energies 3C 445 was detected with the *BeppoSAX*-PDS instrument (Grandi et al. 2006). However, due to the large field of view of the high energy detector onboard *BeppoSAX* and the possible contamination from a nearby cluster (A2440) this observation could provide only a weakly constrained measurement of the reflected continuum. 3C 445 is also detected with the BAT detector on board Swift and is part of the 58 months catalogue[1] (Baumgartner et al. 2010).

In the soft X-ray band the high resolution spectra, accumulated with the XMM-*Newton*-RGS, provided the first tentative detection of the O VII and O VIII emission lines (Grandi et al. 2007). This detection suggested that the soft X-ray emission is produced in a warm gas photoionised by the AGN as observed in Compton-thin Seyfert 2 galaxies (Bianchi et al. 2006; Guainazzi & Bianchi 2007). Recently we obtained a deep *Chandra* observation of 3C 445, which provided the evidence for both emission and absorption from photoionised gas in this obscured AGN and provided the first detailed quantitative measurement. In particular, in the *Chandra* spectrum several soft X-ray emission lines (from the He and H-like transitions of O, Ne, Mg and Si) were detected and resolved. From the ratio of forbidden to intercombination emission lines in the He-like triplets and the velocity broadening ($v_{FWHM} \sim 2600$ km s^{-1}) it was inferred that the photoionised emitter has properties very similar to the Broad Line Region. The *Chandra* spectrum confirmed that 3C 445 is highly obscured but it was suggestive that X-ray absorber could be associated with a disk wind with an observed outflow velocity of 10000 km s^{-1}, which is launched from a sub-parsec scale location.

Here we present the analysis and results from our 140 ks *Suzaku* observation of 3C 445, while the results on the high resolution soft X-ray spectra obtained with our deep (200 ksec) *Chandra* LETG observation are discussed in a companion paper (Reeves et al. 2010). The *Swift*-BAT spectrum ($S/N = 16.2$; $F(14-195) = 4.2 \pm 0.5 \times 10^{-11}$) is used in this paper and fitted jointly with the *Suzaku* data. We took advantage of the *Chandra* results, while modelling the *Suzaku* data (§3.2 and §3.4), and we present a comparison between the two datasets, which provided tentative evidence that the X-ray absorbers varied (§3.4 & §4).

The paper is structured as follows. The observation and data reduction are summarised in § 2. In § 3 we present the modelling of the broad-band spectrum, aimed to assess the nature of the X-ray absorber, the amount of reflection and the iron K emission line properties. Discussion and conclusions follow in §§ 4 and 5. Throughout this paper, a concordance cosmology with $H_0 = 71$ km s^{-1} Mpc^{-1}, Ω_Λ=0.73, and Ω_m=0.27 (Spergel et al. 2003) is adopted.

2 OBSERVATIONS AND DATA REDUCTION

On 25 May 2007 *Suzaku* (Mitsuda et al. 2007) observed 3C 445 for a total exposure time of about 140 ksec (over a total duration of $\sim$ 270 ksec); a summary of observations is shown in Table 1. *Suzaku*

carries on board four sets of X-ray mirrors, with an X-ray CCD (XIS; three front illuminated, FI[2], and one back illuminated, BI) at their focal plane, and a non imaging hard X-ray detector (HXD). All together the XIS and the HXD-PIN cover the 0.5–10 keV and 12–70 keV bands respectively. Data from the XIS (Koyama et al. 2007) and HXD-PIN (Takahashi et al. 2007) were processed using v2.1.6.14 of the *Suzaku* pipeline applying the standard screening[3].

2.1 The Suzaku-XIS analysis

The XIS data were selected in 3×3 and 5×5 editmodes using only good events with grades 0,2,3,4,6 and filtering the hot and flickering pixels with the script *sisclean*. The net exposure times are 108 ksec for each of the XIS. The XIS source spectra were extracted from a circular region of $2.4'$ radius centered on the source, while background spectra were extracted from two circular regions of $2.4'$ radius offset from the source and the calibration sources. The XIS response (rmfs) and ancillary response (arfs) files were produced, using the latest calibration files available, with the *ftools* tasks *xisrmfgen* and *xissimarfgen* respectively. The spectra from the two FI CDDs (XIS 0 and XIS 3) were combined to create a single source spectrum (hereafter XIS–FI), while the BI (the XIS1) spectrum was kept separate and fitted simultaneously. The net 0.5–10 keV count rates are: (0.154 ± 0.001) cts/s, (0.158 ± 0.001) cts/s, (0.142 ± 0.001) cts/s for the XIS0, XIS3 and XIS1 respectively with a net exposure of 108 ks for each XIS. Data were included from 0.4–10 keV for the XIS–FI and 0.4–8 keV for the XIS1 chip; the difference on the upper boundary for the XIS1 spectra is because this CCD is optimised for the soft X-ray band. The background rates in these energy ranges correspond to only 4.5% and 8.1% of the net source counts for the XIS-FI and XIS1 respectively. The net XIS source spectra were then binned to a minimum of 100 counts per bin and χ^2 statistics have been used.

2.2 The *Suzaku* HXD-PIN analysis

For the HXD-PIN data reduction and analysis we followed the latest *Suzaku* data reduction guide (the ABC guide Version 2[4]), and used the rev2 data, which include all 4 cluster units. The HXD-PIN instrument team provides the background (known as the "tuned" background) event file, which accounts for the instrumental Non X-ray Background (NXB; Kokubun et al. 2007). The systematic uncertainty of this "tuned" background model is believed to be 1.3% (at the 1σ level for a net 20 ks exposure).
We extracted the source and background spectra using the same common good time interval, and corrected the source spectrum for the detector dead time. The net exposure time after the screening was 109.5 ks. We then simulated a spectrum for the cosmic X-ray background counts (Boldt 1987; Gruber et al. 1999) and added it to the instrumental one.

3C 445 is detected up to 70 keV at a level of 12.9% above the background corresponding to a signal-to noise ratio $S/N \sim 30$. The net count rate in the 15–70 keV band is 0.052 ± 0.002cts/s (~ 5700 net counts). For the spectral analysis the source spectrum of 3C 445 was rebinned in order to have a signal-to-noise ratio of five in each energy bin. The HXD-PIN spectrum can be fitted with a single power-law ($\Gamma = 2.0 \pm 0.3$); this provides a first estimate of the 15-70 keV flux of about $\sim 3.1 \times 10^{-11}$erg cm^{-2} s^{-1}. The extrapolated flux in the *Swift* band (14-195 keV) is $\sim 5 \times 10^{-11}$erg cm^{-2} s^{-1} and it is comparable to the flux reported in the BAT 58 months catalog (Baumgartner et al. 2010).

Table 1. Summary of the observations used: Observatory, Epoch, Instrument, Total and Net exposure time. For *Suzaku* the total exposure time is not the elapsed time of the observation and it already includes the standard screening for the passage above the SSA anomaly. The net exposure times are after the screening of the cleaned event files.

Mission	DATE	Instrument	$T_{(tot)}$ (ks)	$T_{(net)}$ (ks)
Suzaku	2007-5-25	XIS-FI	139.8	108
Suzaku	2007-5-25	XIS 1	139.8	108
Suzaku	2007-5-25	HXD-PIN	139.8	109.5
Chandra	2009-09-25	ACIS-S LETG	–	43.950
Chandra	2009-09-29	ACIS-S LETG	–	73.720
Chandra	2009-10-02	ACIS-S LETG	–	83.440

2.3 The *Swift*-BAT observation

The BAT spectrum was obtained from the 58-month survey archive, which provides both the spectrum and the long-term online BAT light curve; the data reduction procedure of the eight-channel spectrum is described in (Tueller et al. 2010 and Baumgartner et al. 2010). For the analysis we used the latest calibration response file (the diagonal matrix: diagonal.rsp) provided with the spectrum and we also inspected the light curve that shows no strong variability. The net count rate in the 14–195 keV band is $(4.2 \pm 0.3) \times 10^{-4}$ cts s^{-1}.

2.4 The *Chandra* observation

Recently 3C 445 was observed with the *Chandra* ACIS-S for 200 ksec. The observation was performed on September 2009 with the Low-Energy Transmission Grating (or LETG; Brinkman et al. 2000) in the focal plane. In this paper we concentrate on the *Suzaku* results, while the *Chandra* data reduction, analysis and results are described in a companion paper (Reeves et al. 2010). Thanks to the high sensitivity and spectral resolution the LETG data allowed us to resolve the soft X-ray emission lines, determining the gas density and location. Since 3C 445 is not highly variable either in flux and spectral shape, we were able to take the advantage of the *Chandra* results, while modelling the *Suzaku* data and vice-versa.

3 SPECTRAL ANALYSIS

All the models have been fit to the data using standard software packages (XSPEC ver. 11.3). In the following, unless otherwise

[2] At the time of this observation only XIS0 and XIS3 were still operating
[3] The screening filters all events within the South Atlantic Anomaly (SAA) as well as with an Earth elevation angle (ELV) $< 5°$ and Earth day-time elevation angles (DYE_ELV) less than 20°. Furthermore also data within 256s of the SAA were excluded from the XIS and within 500s of the SAA

3.1 The broad band continuum

Previous X-ray studies of 3C 445 revealed that its X-ray spectrum is complex and cannot be modelled with a single power-law component. This is confirmed by our *Suzaku* observation, where the XIS curved continuum is highly indicative of the presence of strong absorption. A fit to the 0.4–10 keV XIS data with a single redshifted power-law model modified by Galactic ($N_H = 5.33 \times 10^{20} cm^{-2}$; Dickey & Lockman 1990) and intrinsic (in the rest-frame of 3C 445) absorption, yields a poor fit ($\chi^2/dof = 3865.2/388$), with a hard photon index ($\Gamma \sim -0.27$) and leaves strong residuals at low and high energies.

We then added to this model a soft power-law component absorbed only by the Galactic column, which represents the primary X-ray emission scattered into our line of sight. The photon indices of these two power-law components were constrained to be the same. This model is still a poor description the X-ray emission from 3C 445 ($\chi^2/dof = 885.3/387$) and as already noted with the XMM-*Newton* observation (S07) it fails to reproduce the overall curvature, which suggests that a more complex absorber is required. Furthermore, it leaves strong residuals both at the Fe Kα line energy range and in the soft X-ray band and the photon index is found to be hard ($\Gamma \sim 1.3$) with respect to the typical values of radio loud AGN (Sambruna et al. 1999; Reeves & Turner 2000).

We then tested a model for the continuum similar to the best fit found for the XMM-*Newton* data, without including any reflection, and we ignored the 5–7.5 keV band, where the Fe Kα emission complex is expected. The absorber is now modelled with a dual absorber; one fully covering the primary X-ray emission and one only partially covering it. A scattered component, modelled with a second power-law with the same photon index of the primary one is still included. This is now a better representation of the X-ray continuum and the photon index is now steeper ($\Gamma = 1.70 \pm 0.11$). The column densities of the absorbers are found to be $N_{H1} = (1.1 \pm 0.2) \times 10^{23}$ cm^{-2}and $N_{H2} = (3.3 \pm 0.6) \times 10^{23}$ cm^{-2}, for the fully and partial covering absorber respectively; the covering fraction of the latter absorber is $f_{cov} = 0.79^{+0.06}_{-0.08}$, while the scattering fraction is found to be $f_{scatt} \sim 0.03$.

This continuum model is still too simple with respect to the broad band X-ray emission, indeed its extrapolation under-predicts the counts collected above 10 keV (see Fig. 1). Furthermore, as seen with XMM-*Newton* this model leaves strong line-like residuals at the energy of the Fe Kα emission line. These residuals suggest the presence of a strong narrow core at the expected energy of the Fe Kα line (6.4 keV) and a possible weak component red-ward the narrow core at $E \sim 6$ keV (observed frame), which could be identified with the Compton shoulder (see Fig. 2). Both these features and the hard excess seen in the spectrum above 10 keV suggest the presence of a strong reflection component. The presence of this latter component was already suggested with the previous *BeppoSAX* observation (Dadina 2007; Grandi et al. 2006), however taking into account the possible contamination from a nearby cluster of galaxies (A2440, z=0.094) it was not possible to derive strong constraints on it.

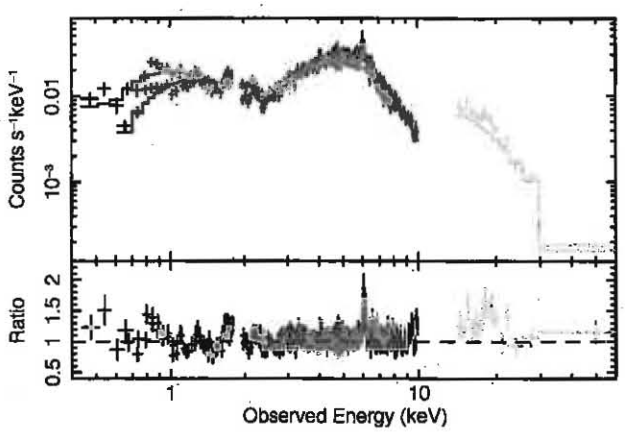

Figure 1. Suzaku 0.4–60 keV spectra (in the electronic version: XIS-FI, black; XIS1, red; HXD-PIN green) of 3C 445; data have been rebinned for plotting purposes. The upper panel shows the data and the dual absorber model ($\Gamma \sim 1.7$; $N_{H1} \sim 10^{23}$ cm^{-2}; $N_{H2} \sim 3.3 \times 10^{23}$ cm^{-2}), fitted over the 0.4–5 keV and 7.5–10 keV band. The lower panel shows the data/model ratio to this model. Clear residuals are visible at the iron K-shell energy band and in the HXD-PIN energy range. The excess of counts in the HXD-PIN spectrum compared to the XIS, is probably due to the Compton reflection hump.

We set the cross-normalization factor between the HXD and the XIS-FI spectra to 1.16, as recommended for XIS nominal observations processed after 2008 July (Manabu et al. 2007; Maeda et al. 2008[5]), and allowed the cross-normalization of the *Swift*-BAT data to vary, since the two observations are not simultaneous.
We included in the model the Fe Kα line and a Compton reflection component. At this stage this component was modelled with the PEXRAV model in Xspec (Magdziarz & Zdziarski 1995), with the abundances set to solar values and the inclination angle i to 60°. We note that the cluster A2440, which was thought to contaminate the X-ray emission detected with the *BeppoSAX*-PDS instrument lies at the edge of the FOV of the HXD-PIN and thus the contamination from it should be minimal. The cross-normalization with the Swift data is consistent with one as indicated by the similar HXD and BAT fluxes ($C \sim 0.8$), furthermore the slope of the *Swift*-BAT spectrum is consistent with the HXD-PIN data, with no evidence of a high-energy cutoff. The similarity in flux and shape confirm that the *Suzaku* HXD-PIN spectrum is dominated by the emission of 3C 445 with no or minimal contamination from the nearby cluster. It is worth noting that since the *Swift*-BAT data allow us to extend the analysis only up to 150 keV, we cannot discriminate if the lack of any roll over is real or simply due to the still limited bandpass and the complex curvature of the spectrum. Indeed upon leaving the high energy cutoff free to vary we can set only a lower limit ($E > 60$ keV).

The amount of reflection, defined by the subtending solid angle of the reflector $R = \Omega/2\pi$ is found to be $R \sim 1.1 \pm 0.4$, while the parameters of the absorbers are consistent with the values obtained with the previous model ($N_{H1} = 1.1^{+0.1}_{-0.1} \times 10^{23}$ cm^{-2} and $N_{H2} = 3.2^{+0.4}_{-0.4} \times 10^{23}$ cm^{-2}, $f_{cov} = 0.74^{+0.02}_{-0.02}$ and $\chi^2/dof = 496.7/408$). The photon index is now $\Gamma = 1.78^{+0.08}_{-0.07}$. The Fe K$\alpha$ emission line is centered at $E = 6.384 \pm 0.012$ keV,

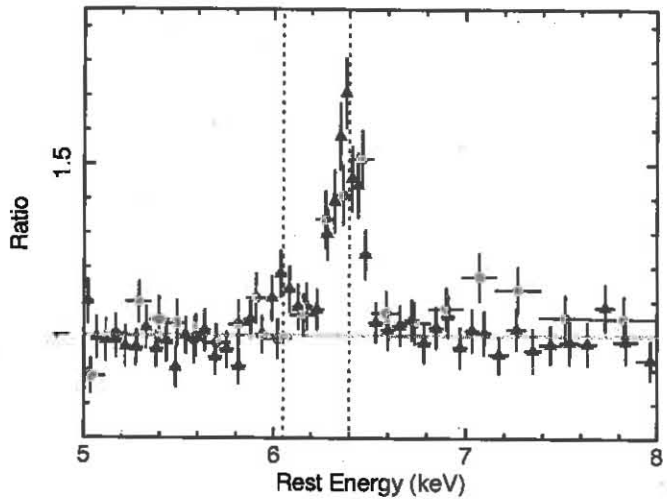

Figure 2. Data/model ratio between the XIS data (XIS-FI, black triangles in the electronic version; XIS-BI red open circles in the electronic version) and the dual absorber model showing the iron line profile. The data clearly show (indicated by the two vertical lines) a narrow core at 6.4 keV (rest frame), and a weak narrow emission feature at$\sim$ 6.1 keV (rest frame).

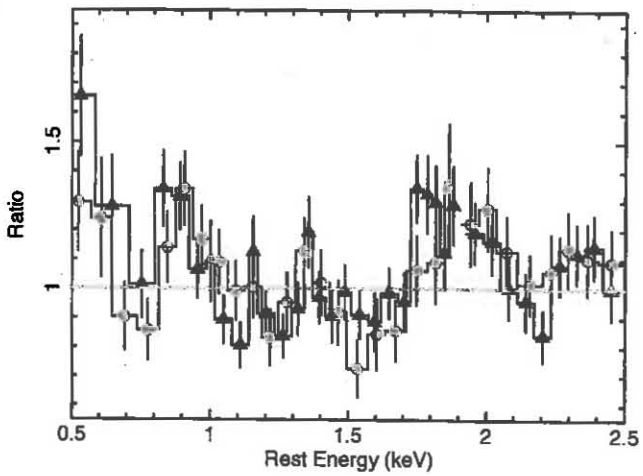

Figure 3. Zoom on the 0.5–2.5 keV range of the data/model ratio to a power-law component ($\Gamma \sim 1.7$; XIS-FI, black triangles in the electronic version; XIS-BI open red circles in the electronic version). Several emission lines are clearly present in the residuals.

it has an equivalent width of $EW = 105 \pm 15$ eV with respect to the observed continuum and it is has a measured width of $\sigma = 37 \pm 34$ eV. We note that the inclusion of the reflection component is not only statistically required ($\Delta\chi^2 = 23$ for 1 dof or $\chi^2/dof = 520.1/409$), but also its strength is consistent with the observed EW of the Fe Kα emission line. This model gives a 2–10 keV observed flux of $\sim 7 \times 10^{-12}$ erg cm^{-2} s^{-1} and a intrinsic (corrected for absorption) luminosity of $\sim 1.2 \times 10^{44}$ erg s^{-1}, which is similar to the value measured with XMM-*Newton* and *ASCA* .

This model now provides a better phenomenological description 3C 445's X-ray continuum, however statistically the fit is still poor ($\chi^2/dof = 496.7/408$), with some residuals in the 2–10 keV band, suggesting that this model is still too approximate for the broad band emission of 3C 445. Several line like residuals are present at $E < 2$ keV, in agreement with the previous detection from *ASCA* and XMM-*Newton* (Sambruna et al. 1999, 2007; Grandi et al. 2007). Finally we note that without the inclusion of the *Swift*-BAT, the overall statistics ($\chi^2/dof = 491.7/401$) and parameters, derived with this simple and phenomenological model, are similar ($\Gamma = 1.79^{+0.09}_{-0.08}$ and $R \sim 1.2 \pm 0.5$). The reflection component is also statistically required with the *Suzaku* data alone ($\Delta\chi^2 = 21$ for 1 dof or $\chi^2/dof = 513/402$). A more detailed description of the modelling of the Fe Kα emission line and of the overall hard X-ray spectral curvature is provided in the sections 3.3 and 3.4; nevertheless we note that this modelling does not strongly affect the results of the soft X-ray emission, which are presented in the following section.

3.2 The soft X-ray spectrum

In order to model the soft X-ray emission, we allow the photo-instrument several lines from O, Ne, Mg and Si are clearly detected (see Fig. 3; black and red data points). Taking into account the lower count statistics of the soft X-ray spectrum, we decided to use a finer binning for the XIS data adopting a minimum of 50 counts per bin. The fit statistic of the continuum model is now $\chi^2/dof = 746.4/676$. We first added to the continuum model several narrow ($\sigma = 10$ eV) Gaussian lines, allowing also all the continuum parameters to vary; overall upon including 6 lines the fit statistic improves and it is now $\chi^2/dof = 662.8/676$ ($\Delta\chi^2 = -83$ for 12 dof). We note that the Γ of the soft power-law is now similar to the primary power-law component, we thus constrained the two photon indices to be the same.

In Table 2, we list all the detected lines with their properties, statistics and possible identification, which point toward emission from lighter elements in particular $2 \rightarrow 1$ transition of H- and He-like O, Mg and Si. Though some of the soft X-ray emission lines are not detected with high statistical significance (e.g. for Mg XI we have $\Delta\chi^2 = 5.2$), their detection and interpretation is in agreement with the results obtained with the deep *Chandra* LETG observation (Reeves et al. 2010). The *Chandra* spectrum confirms the identification of the feature detected at $\sim$0.88 keV with O VIII RRC. This feature, along with the OVII RRC at $E \sim 0.74$ keV, are resolved by the *Chandra* LETG and have measured widths which imply that the emitting gas is photo- rather than collisionally-ionised.

Since with the *Suzaku* XIS CCD resolution, we cannot resolve the line triplets and we cannot establish with high accuracy the identification of some of the lines, and taking into account that 3C 445 is not highly variable, we adopted for the soft X-ray emission the best fit model obtained with the *Chandra* LETG data. This model includes two grids of photoionized emission models (with $\log \xi_1 \sim 1.82$ erg cm s^{-1} and $\log \xi_2 \sim 3.0$ erg cm s^{-1}) generated by XSTAR (Kallman et al. 2004), which assumes a $\Gamma \sim 2$ illuminating continuum and a turbulence velocity of $\sigma_v = 100$ km/s and a column density for the emitter of $N_H = 10^{22}$cm^{-2}. We note that

Table 2. Summary of the soft-X-ray emission lines. The energies of the lines are quoted in the rest frame. Fluxes and possible identifications are reported in column 2 and 3. For the emission feature detected at ~ 0.88 keV the alternative identifications are reported in brackets. The EW are reported in column 4 and they are calculated against the total observed continuum at their respective energies. In column 5 the improvement of fit is shown; the value for the model with no lines is $\chi^2/dof = 746.4/676$. In column 6 we report the theoretical value for the transitions. The Γ of the soft power-law is tied to the hard power-law component. We note that some of the soft X-ray emission lines are not detected with high statistical significance (e.g for Ne X Lyα and Mg XI Heα we have $\Delta\chi^2 = 7.7$ and $\Delta\chi^2 = 5.2$, respectively).

Energy (keV) (1)	Flux (10^{-6}ph cm^{-2} s^{-1}) (2)	ID (eV) (3)	EW (eV) (4)	$\Delta\chi^2$ (5)	E_{Lab} (keV) (6)
$0.54^{+0.03}_{-0.02}$	$15.92^{+0.72}_{-0.70}$	O VII Heα	$47.6^{+22.3}_{-20.6}$	10.85	0.561(f); 0.569 (i); 0.574(r)
$0.88^{+0.02}_{-0.02}$	$7.37^{+1.98}_{-2.22}$	O VIII RRC (Fe XVIII-XIX)	$51.0^{+13.8}_{-14.5}$	30.0	> 0.873 0.853-0.926
$0.99^{+0.01}_{-0.03}$	$2.85^{+1.45}_{-1.62}$	Ne X Lyα	$24.0^{+12.2}_{-13.6}$	7.7	1.022
$1.36^{+0.03}_{-0.03}$	$1.40^{+0.78}_{-1.14}$	Mg XI Heα	$19.5^{+11.0}_{-15.8}$	5.2	1.331(f); 1.343(i); 1.352 (r)
$1.80^{+0.03}_{-0.03}$	$2.89^{+1.31}_{-0.46}$	Si XIII Heα	$59.9^{+27.1}_{-9.6}$	20.7	1.839(f); 1.853(i); 1.867 (r)
$2.33^{+0.05}_{-0.04}$	$1.65^{+0.76}_{-0.75}$	S I Kα	$45.7^{+21.1}_{-20.7}$	9.2	2.307

fixed to the one adopted with the *Chandra* LETG analysis. We applied this best fit model to the XIS soft spectrum, keeping the abundances fixed to the values measured with the LETG spectrum and allowing only the normalisations and the photon index to vary. This model is now a good description of the soft spectrum ($\chi^2/dof = 696.6/674$) and no strong residuals are present below 3 keV. As a final test, we allowed the ionisation parameter of the two emitters to vary and found a good agreement between the *Suzaku* and *Chandra* best-fit ($\log \xi_1 = 1.95^{+0.14}_{-0.08}$ erg cm s^{-1} and $\log \xi_2 = 3.17^{+0.21}_{-0.23}$ erg cm s^{-1}). We note that the presence of the higher ionisation emitter is not statistically required ($\Delta\chi^2 = 3$), and a good fit is found with a single zone with $\log \xi = 1.97^{+0.24}_{-0.12}$ erg cm s^{-1}. We note also that there is still a line like residual at ~ 2.3 keV, which cannot be modelled with these two components. We thus included in the model an additional Gaussian line, the line is found to be $E = 2.33 \pm 0.05$ keV and could be associated with S $K\alpha$. Finally, we note that both the ionisation parameters and the fluxes of the ionised emitters measured with *Suzaku* are consistent with the one measured with the *Chandra* LETG data.

The extraction region of the *Suzaku* XIS spectra includes the Narrow Line QSO (1WGA J2223.7-0206), which was firstly detected by ROSAT and which is located at about 1.3' from the 3C 445. Its X-ray spectrum obtained with XMM-*Newton* was analysed and discussed by Grandi et al. (2004). The observed X-ray flux (F (0.2-10 keV)$\sim 3 \times 10^{-13}$erg cm^{-2} s^{-1} , with 80% emitted below 2 keV) was found to be comparable in the soft X-ray band to the emission of 3C 445 and could thus, in principle, strongly affect the *Suzaku* spectrum.

We note however that a contemporaneous *Swift* observation (of about 10 ks) of 3C 445 did not detect 1WGA J2223.7-0206 in the field of view of the *Swift*-XRT, suggesting that 1WGA J2223.7-0206 was much fainter during the Suzaku observation. We estimated an upper limit on its soft X-ray flux of $(0.5-2)$ keV $\sim 2.3 \times 10^{-13}$erg cm^{-2} s^{-1} for the *Chandra* and *Suzaku* observation respectively. This suggests that the X-ray emission of 1WGA J2223.7-0206 was not comparable to 3C 445, indeed the the roll angle of the *Chandra* observation of 3C 445 was specifically set in order to avoid the contamination from Narrow Line QSO.

As a last check, we searched also the *Chandra* source catalog (Evans et al. 2010) and the Chandra XAssist source list (Ptak & Griffiths 2003) for X-ray bright sources within the XIS extraction radius. Three sources are detected with a 0.3–8 keV flux greater than 9×10^{-15}erg cm^{-2} s^{-1} and 1WGA J2223.7-0206 is the brightest among them with a 0.5–8 keV flux of about 5×10^{-14}erg cm^{-2} s^{-1} . Thus we inspected the *Chandra* ACIS-S spectrum of 1 WGA J2223.7-0206, which has ~ 300 net counts. In order to derive an estimate of the soft X-ray flux, we fitted the *Chandra* data with a single absorbed power law component ($\Gamma \sim 1.7$, $N_H \sim 3 \times 10^{21}$ cm^{-2}). We found that also during the *Chandra* observation 1WGA J2223.7-0206 was fainter than during the XMM-*Newton* pointing and its 0.5–2 keV observed flux was 1.6×10^{-14}erg cm^{-2} s^{-1} . We thus conclude that the contamination of this second AGN is minimal.

3.3 Modelling the Fe Kα line and the high energy emission

We then considered the hard X-ray emission of 3C 445 using for the soft X-ray emission a single photoionised plasma plus a Gaussian emission line at ~ 2.33 keV as described above and keeping the ionisation parameter fixed to the best fit value. For the remainder of the analysis we used again the XIS data grouped with a minimum of 100 counts per bin. We examined simultaneously the *Suzaku* XIS (0.4–10 keV) and HXD-PIN data (15.– 65. keV) and the *Swift*-BAT, setting the cross-normalization factor between the HXD and the XIS-FI spectra to 1.16, and allowing

As shown in Fig. 2 the residuals at the energy of the Fe K band clearly reveal the presence of a strong narrow core at the expected energy of the Fe Kα line (6.4 keV), while no clear residuals are present at the energy of the Fe Kβ line. To model the Fe Kα line we first added a narrow Gaussian line at the energies of Fe Kα; the inclusion of the line in the model improves the fit by $\Delta\chi^2 = 101$ for 3 degrees of freedom ($\chi^2/dof = 456.3/405$). The Fe Kα core has an equivalent width of $EW = 100 \pm 14$ eV with respect to the observed continuum, it is centered at $E = 6.383 \pm 0.012$ keV and has a measured width of $\sigma = 34 \pm 30$ eV. As suggested by the residuals a Fe Kβ is not statistically required, however we found that the upper limit on its flux is 13.6% of the Fe Kα line flux, consistent with the theoretical value. The amount of reflection ($R = 0.9 \pm 0.4$) is found to be consistent with the observed EW of the Fe Kα line, for an inclination angle $i = 60°$ and $\Gamma \sim 1.8$.

Finally, we note that in the XIS-FI data, there are still some line-like residuals red-wards the Fe Kα line. Upon adding a second narrow Gaussian line the fit only marginally improves ($\chi^2/dof = 445.1/403$ corresponding to $\Delta\chi^2 = 11$ for 2 dof), significant at 99.6% confidence from the F-test. If this emission line is real the closest candidate for this feature could be the Compton shoulder to the Fe Kα line. We note however that its energy ($E = 6.05 \pm 0.11$ keV) is slightly lower than the expected value of the first scattering peak (E$\sim$ 6.24 keV). An alternative possibility is that this line is a redwing of a possible relativistic disk-line. Thus we replaced the Gaussian with relativistic diskline component (DISKLINE in XSPEC; Fabian et al. 1989); this code models a line profile from an accretion disk around a Schwarzschild black hole. The main parameters of this model are the inner and outer radii of the emitting region on the disk, and its inclination. The disk radial emissivity is assumed to be a power-law, in the form of r^{-q}. For the fit we fixed the emissivity $q = 3$ and the angle to 60°. The fit statistic is similar to the Gaussian profile ($\chi^2/dof = 446.6/402$), and we found that the best fit parameters of this diskline corresponds to emission from an annulus at ~ 100 R_g (with $R_g = GM/c^2$) and with an EW= 75 ± 40 eV. The energy of this putative line, although not well constrained, is consistent with the ionised Fe line ($E = 6.64 \pm 0.16$ keV). Given, the lower statistical significance and the uncertainties on the energy centroid of this possible emission line, we will not discuss it any further.

We then replaced the PEXRAV and Gaussian components with a more updated model for the Compton reflection off an optically-thick photoionized slab of gas, which includes the Fe K emission line (REFLIONX; Ross & Fabian 2005; Ross et al. 1999). We assumed Solar abundances, and we found the fit is equally good ($\chi^2/dof = 453.8/405$). As expected the ionisation of the reflector is found to be low, $log\xi < 1.74$ erg cm s^{-1}, in agreement with the measured energy centroid of the iron Kα emission line being close to the value for neutral iron (or less ionised than Fe XVII). We thus fixed the ionisation parameter to $\xi = 10$ erg cm s^{-1}, which is the lower boundary for the REFLIONX model. We note that the residuals at ~ 6.05 keV are still present, we thus keep in the model the additional redshifted emission line. The parameters of the absorber

Table 3. Summary of the neutral partial covering absorber model. [a]The ionisation of the reflector has been fixed to the minimum value allowed by the model; if left free to vary the upper limit is found to be 55 erg cm s^{-1}. The ionisation parameters of the soft X-ray plasma is fixed to $\log \xi = 1.97$ erg cm s^{-1}. Fluxes are corrected only for Galactic absorption, while the luminosities are corrected for rest frame absorption.

Model Component	Parameter	Value
Power-law	Γ	$1.74^{+0.06}_{-0.05}$
	Normalisation	$3.82^{+0.63}_{-0.48} \times 10^{-3}$
Scattered Component	Normalisation	$9.9^{+0.5}_{-0.5} \times 10^{-5}$
Absorber	N_{H1}	$1.0^{+0.1}_{-0.2} \times 10^{23}$ cm^{-2}
Absorber	N_{H2}	$3.2^{+0.3}_{-0.3} \times 10^{23}$ cm^{-2}
	f_{cov}	$0.78^{+0.02}_{-0.01}$
Ionised reflection	ξ	10^a erg cm s^{-1}
	Normalisation	$1.20^{+0.12}_{-0.13} \times 10^{-5}$
Ionised emission	Normalisation	$2.2^{+0.6}_{-0.6} \times 10^{-6}$
	χ^2/dof	454/406
	$F_{(0.5-2)keV}$	2.71×10^{-13}erg cm^{-2} s^{-1}
	$F_{(2-10)keV}$	7.01×10^{-12}erg cm^{-2} s^{-1}
	$L_{(0.5-2)keV}$	7.1×10^{43}erg s^{-1}
	$L_{(2-10)keV}$	1.2×10^{44}erg s^{-1}
	$L_{(14-150)keV}$	3×10^{44}erg s^{-1}

3.4 The X-ray absorber

Assuming that the absorber is neutral the broadband X-ray emission of 3C 445 requires the presence of two absorbers one fully covering and one only partial covering. The best fit parameters of this model, which we now consider our best-fit neutral absorber model, are listed in Table 3. This dual absorber plus reflection model is a good phenomenological description of the broad band X-ray emission of 3C 445 ; however it may be too simple an approximation of a more complex absorber. We note also that, taking into account the optical classification of 3C 445 as type 1 AGN, the X-ray absorber is not likely to be a neutral absorber covering a large fraction of the nuclear source as derived with the above model. A possibility is that the absorber is mildly ionised and thus it is partially transparent and not efficient in absorbing the optical and soft X-ray emission.

To test this scenario, we then replaced both the partial and the fully covering neutral absorbers with a photoionised absorber, the latter is made using a multiplicative grid of absorption model generated with the XSTAR code (Kallman et al. 2004). For simplicity we modelled the possible relativistic emission line with an additive Gaussian component and we allowed to vary the Galactic absorption ($N_H = (0.63^{+0.22}_{-0.23}) \times 10^{21}$ cm^{-2}). At first we assumed a zero outflow velocity of the absorber and we tested a single zone of absorption. The absorber is found to be mildly ionised ($log\xi = 1.10^{+0.10}_{-0.24}$ erg cm s^{-1}) and with a column density similar to the neutral absorber $N_H = (1.89^{+0.09}_{-0.06}) \times 10^{23}$ cm^{-2}. We note also that the fit marginally improves with respect to the neutral absorber ($\chi^2/dof = 443.1/406$) and overall the model is able to reproduce the curvature of the spectrum. The best fit parameters of this model are listed in Table 4.

A similar ionised absorber was also found with the *Chandra* observation ($log\xi \sim 1.4$ erg cm s^{-1}, $N_H \sim 1.85 \times 10^{23}$

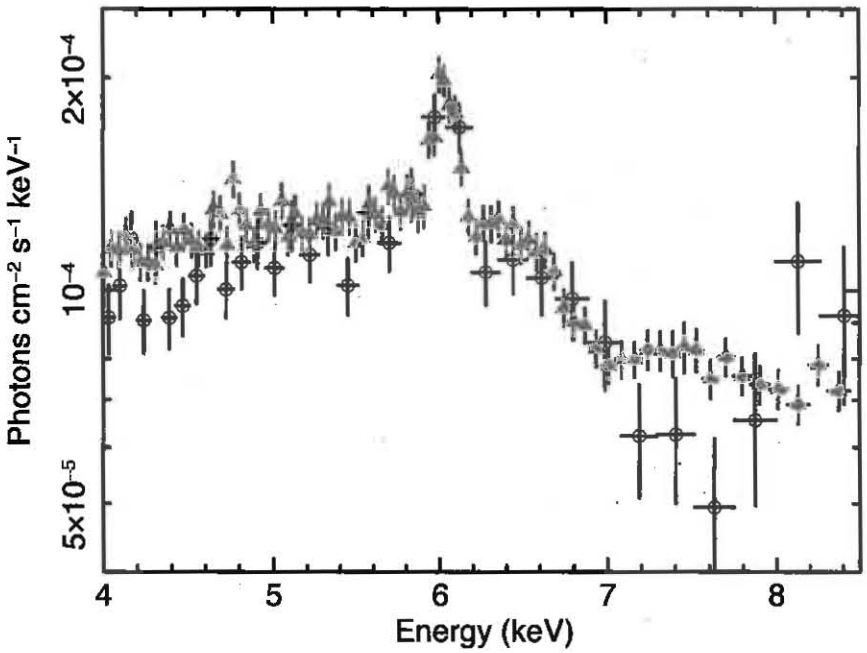

Figure 4. *Chandra* (black circles in the electronic version) and *Suzaku* XIS-FI (red triangles in the electronic version) spectra in the 4–8.5 keV band folded against a simple power law continuum with the normalisations free to vary. In the high energy part, the spectra show a sharper absorption feature in *Chandra* spectrum compared to a more shallow and possibly broader drop in the *Suzaku* data.

Table 4. Summary of the ionised absorber model. [a]The ionisation of the reflector has been fixed to the minimum value allowed by the model. Fluxes are corrected only for Galactic absorption, while the luminosity are corrected for rest frame absorption. The ionisation of the emitter has been fixed to best fit value.

Model Component	Parameter	Value
Power-law	Γ	$1.85^{+0.05}_{-0.04}$
	Normalisation	$4.79^{+0.42}_{-0.69} \times 10^{-3}$
Scattered Component	Normalisation	$10.2^{+0.6}_{-0.6} \times 10^{-5}$
Absorber	N_{H1}	$1.89^{+0.09}_{-0.06} \times 10^{23}$ cm^{-2}
	$log\xi$	$1.10^{+0.10}_{-0.24}$ erg cm s^{-1}
Ionised reflection	ξ	10^{a} erg cm s^{-1}
	Normalisation	$1.26^{+0.15}_{-0.14} \times 10^{-5}$
Ionised emission	Normalisation	$2.4^{+0.8}_{-0.7} \times 10^{-6}$
	χ^2/dof	443/406
	$F_{(0.5-2)keV}$	2.86×10^{-13}erg cm^{-2} s^{-1}
	$F_{(2-10)keV}$	7.03×10^{-12}erg cm^{-2} s^{-1}
	$L_{(0.5-2)keV}$	8.5×10^{43}erg s^{-1}
	$L_{(2-10)keV}$	1.3×10^{44}erg s^{-1}
	$L_{(14-150)keV}$	3×10^{44}erg s^{-1}

($\Delta C = 22$, Reeves et al. 2010). Thus we allowed the absorber to be outflowing, but this does not statistically improve the fit ($\Delta\chi^2 = 2$). The parameters of this absorber (N_H and $log\xi$) are found to be similar to the case with no net velocity shift and albeit it is not well constrained the outflowing velocity is found to be slightly lower than the *Chandra* one ($v_{out} < 0.01c$).

To further investigate the apparent discrepancy between the *Chandra* and *Suzaku*'s results we performed a joint fit of the two observations. Though the source is not highly variable we the *Suzaku* observation ($\sim$ 10%). As seen with the independent fit the N_H and $log\xi$ of the ionised absorbers are found to be consistent within the two observations ($\Gamma \sim 1.73^{+0.22}_{-0.19}$, $N_H \sim 1.85^{+0.09}_{-0.11} \times 10^{23}$ cm^{-2}, $\xi \sim 1.4^{+0.20}_{-0.12}$ erg cm s^{-1}and $\Gamma \sim 1.85^{+0.05}_{-0.04}$, $N_H \sim 1.89^{+0.09}_{-0.06} \times 10^{23}$ cm^{-2}, $\xi \sim 1.1^{+0.10}_{-0.24}$ erg cm s^{-1}from the *Chandra* and *Suzaku* best fit respectively; see also Table 3 of Reeves et al. 2010) but not the outflowing velocities. The comparison between the *Chandra* and *Suzaku* data is shown in Fig. 4; in the *Suzaku* data the drop at high energies appears to be broader and less deep. We note that there is also a possible hint of a higher curvature of the *Chandra* spectrum, indeed the *Chandra* spectrum is below the *Suzaku* data also between 4–6 keV. This could be a signature of a variation of the X-ray absorber, being less transparent during the *Chandra* observation. As we show below, with the present data and taking into account the complexity of the model we cannot confirm or rule out a modest variability of the absorber.

As a final check we inspected the previous XMM-*Newton* observation, indeed also in that observation there was a hint of a possible absorption feature at 6.9 keV (Sambruna et al. 2007), though the underlying continuum shape was slightly different. In particular, lacking the high energy data, the amount of reflection could not be constrained. Taking into account, that the source did not strongly vary (in shape and flux), between the two observations, we then simultaneously fitted the XMM-*Newton* and *Suzaku* spectra allowing the cross-normalization to vary and we tested a single ionised absorber (with no outflowing velocity). We found that the XMM-*Newton* spectrum is remarkably in agreement with the *Suzaku* one. In particular we note that the residuals are

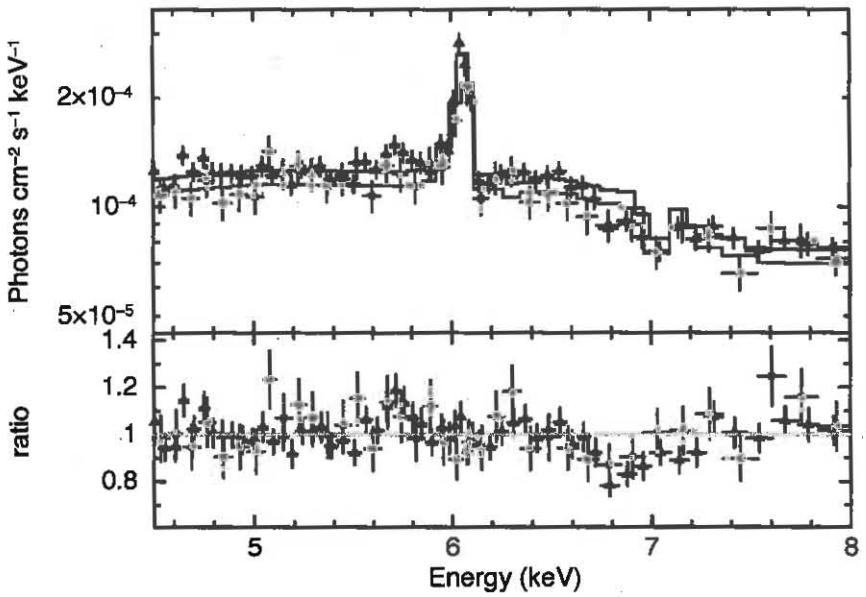

Figure 5. Upper panel: *Suzaku* XIS-FI (filled triangles, black in the electronic version), XMM-*Newton* EPIC-pn (filled squares, red in the electronic version) band folded against a single mildly ionised absorber model with the outflowing velocity fixed to the *Chandra* best-fit value. Lower panel: data/model ratio to the above single ionised absorber. The XIS-FI and EPIC-pn residuals are consistent with each other. They both show a deficit of counts around $\sim$ 6.8 keV (observed frame, corresponding to $\sim$ 7.2 keV in the rest-frame).

redwing of a relativistic Fe Kα line.

Two possible scenarios could explain the observed differences between the *Suzaku* and the *Chandra* observations, the first is that the absorber has indeed varied, with a lower ionisation and outflowing velocity during the *Suzaku* pointing. A second possibility is that the broader drop seen in *Suzaku* is due to the presence of a more complex and possibly multi-phase absorber. In order to test the second scenario we fixed the outflowing velocity of the ionised absorber to the one seen with the *Chandra* observation. The fit is statistically worse ($\chi^2 = 496.7/406$ corresponding to a $\Delta\chi^2 = 53$) and clear residuals are present, both in the XMM-*Newton* and *Suzaku* spectra, at $\sim$ 7.2 keV ($\sim$ 6.8 keV in the observed frame), which are reminiscent of a possible absorption feature. Indeed, the *Chandra* absorption feature appears to be slightly narrower and more blueshifted, compared to the drop in the *Suzaku* data. Forcing the low ionisation absorber fitted to the *Suzaku* data to have the same outflow velocity as inferred from the *Chandra* observation, then results in a deficit of counts around 7 keV (observed frame) in the *Suzaku* and XMM-*Newton* spectra, when compared to the *Chandra* model (see Fig. 5).

The deficit could then be modelled with an additional absorption line in the Suzaku data, perhaps arising from a higher ionisation absorber. As a first test, using only the *Suzaku* data, we included in the model an additional inverted Gaussian, statistically the fit is similar with respect to the single ionised absorber with no outflow velocity ($\chi^2/dof = 450.9/403$). The energy of this line is found to be $E = 7.30 \pm 0.05$ keV (6.9 keV in the observed frame) and the $EW = 62^{+23}_{-22}$eV, which would imply a column density of the absorber of about $N_H \sim 10^{23}$cm^{-2}. The closest candidate for this absorption feature is the $1 \rightarrow 2$ transition transition of Fe XXVI ($E = 6.97$ keV) blueshifted by $v \sim 0.05\ c$, while if the absorption

We then tested a more complex model for the absorber including a second ionised absorber and leaving free to vary the outflow velocity of this absorber, while the outflow velocity of the mildly ionised absorber was fixed to best fit value found with *Chandra* ($v = 0.034c$). As for the mildly ionised absorber we used a grid created with XSTAR, for this grid we assumed again solar abundances, a $\Gamma \sim 2$ illuminating continuum and, taking into account the apparent broadening of the absorption feature, we assumed a turbulent velocity of 3000 km s^{-1}. The addition of this second absorber does not statistically improve the fit with respect to the scenario with a single ionised absorber with no net velocity shift ($\chi^2/dof = 453/403$). This absorber if found to be fast outflowing $v \sim 0.04c$, highly ionised log $\xi > 4.7$ erg cm s^{-1}and high column density $N_H \sim 10^{24}$ cm^{-2} ($N_H = 2.8^{+0.8}_{-2.6} \times 10^{24}$ cm^{-2}). It is important to note that the significance of this second absorber is hindered by the choice of the underlying continuum model and more importantly by the choice of outflow velocity of the mildly ionised absorber.

The simplest interpretation is that there is a modest variability of the mildly ionised absorber, while we cannot rule out the presence of a second highly ionised absorber. To distinguish between these scenarios we need higher spectral resolution observations, such as the one that will be provided with the ASTRO-H calorimeter.

4 DISCUSSION AND CONCLUSIONS

To summarise the *Suzaku* data confirm the complexity of the X-ray emission of 3C 445. The soft X-ray spectrum is dominated by several emission lines, which require the presence of at least one ionised emitter with $log\xi \sim 1.97$ erg cm s^{-1}and which is

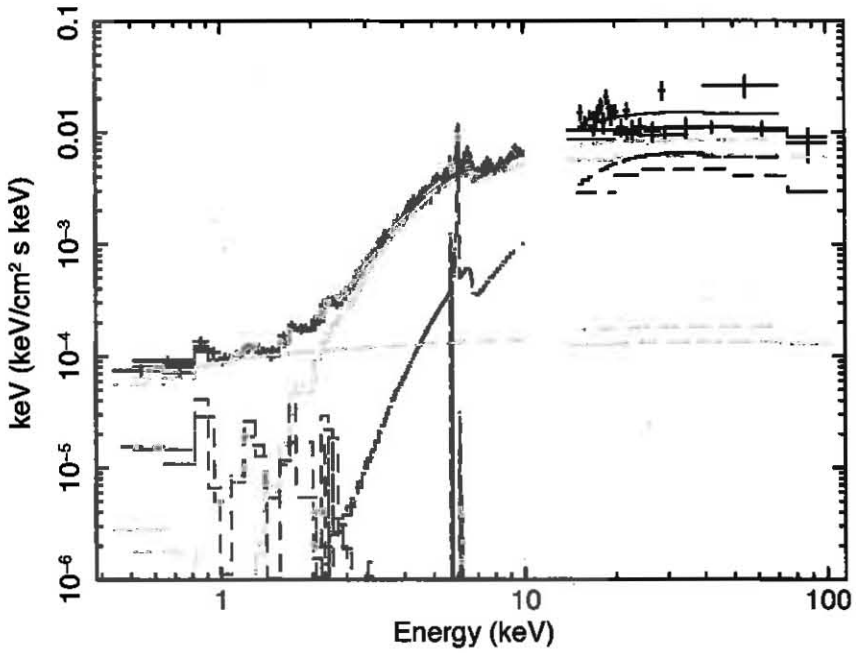

Figure 6. Suzaku and Swift-BAT spectra (black data points) of 3C 445. Data have been rebinned for plotting purposes. The AGN continuum model is composed of a primary power-law component transmitted trough an ionised absorber and a scattered power-law component. The narrow Fe Kα line and the reflection component are modelled with the reflionx model. The possible relativistic component is modelled with a single redshifted Gaussian line. The soft X-ray emission lines are accounted for with an ionised emitter.

which could be either a neutral partial covering absorber or a mildly ionised absorber. Independently from the model assumed for the absorber, the broadband *Suzaku* spectrum allowed us to detect a relatively strong reflection component.

Overall, the X-ray spectrum of 3C 445 is remarkably similar to a Seyfert 2, which could be at odds with its classification as a type 1 AGN. The main characteristics resembling a Seyfert 2 are the presence of soft X-ray emission lines as well as the presence of a high column density X-ray absorber. As we will discuss in the next sections two competitive scenarios could explain the X-ray emission of 3C 445, both requiring that our line of sight is not completely blocked towards the central engine since we have evidence that we can see the emission from the Broad Line Regions (Eracleous & Halpern 1994). We will show that our deep *Suzaku* observation combined with a recent *Chandra* observation, with the high-resolution grating LETG, strongly suggest that both the absorption and the soft X-ray lines originate within the putative torus and we are not seeing the source through a uniform and cold absorber.

4.1 The Soft X-ray emission, similarity and differences to Seyfert 2s

The *Suzaku* spectrum confirms the presence of several soft X-ray emission lines, as previously detected with the XMM-*Newton* observation, from Oxygen, Neon, Magnesium and Silicon. In particular, we detected a line at $\sim$ 0.88 keV, which if associated with the O VIII RRC would strongly implies emission from a photoionized plasma as seen in Compton-thin Seyfert galaxies two ionised emitters, with ionisation levels within the range of obscured radio-quiet AGN (Guainazzi & Bianchi 2007).

The limited spectral resolution of the XIS data does not allow us to resolve the lines, thus using only the *Suzaku* data we cannot measure the density of this plasma and place strong constraints on the location of the emitter. However, as 3C 445 is rather constant in flux, we could use the results obtained with the long *Chandra* LETG observation, indeed assuming the same abundances we found that the soft X-ray emission can be similarly described with two ionised emitters with the same ionisation (log $\xi_1 \sim 1.95$ erg cm s^{-1} and log $\xi_2 \sim 3.17$ erg cm s^{-1}) and luminosity as during the *Chandra* observation. The *Chandra* data provided also the first measurement of the densities ($n_e > 10^{10}$ cm^{-3}) and distance ($R \sim 0.01 - 0.1$ pc; Reeves et al. 2010) of these soft X-ray emitters, which are suggestive of a location within the putative torus and reminiscent of the Broad Line Region (BLR). Furthermore, in the *Chandra* data several lines were resolved into their forbidden and intercombination line components, and the velocity widths of the O VII and O VIII emission lines were determined ($v_{\rm FWHM} \sim 2600$ km s^{-1}). Assuming Keplerian motion, this line broadening implies an origin of the gas on sub-parsec scales (Reeves et al. 2010). 3C 445 is not an isolated example, indeed there are other well known cases of Seyfert 1s where the soft X-ray emission lines appear to be produced in the BLR (e.g. MKN 841, Longinotti et al. 2010; Mrk 335, Longinotti et al. 2008, NGC4051, Ogle et al. 2004; NGC 5548, Steenbrugge et al. 2005).

Thus the emerging scenario is that the soft X-ray emission 3C 445 is not produced in a region coincident with the optical

classification as a type 1 AGN, suggests that our line of sight toward the BLR is not completely blocked by a high column density absorber. This photoionized emitter also resembles the "warm gas" observed in more than 50% radio quiet Seyferts 1 (Crenshaw et al. 2003), which acts as a "warm mirror" and at the same time intercepts the line of sight producing absorption features. As we will discuss below these photoionized clouds that we are seeing in emission might be associated with the absorber responsible for the curvature of the X-ray continuum.

4.2 The X-ray absorber/reflector: a distant reflector?

The *Suzaku* spectrum, and in particular the data above 10 keV, allow us to confirm the presence of a strong reflection component and for the first time to provide a measurement of its intensity. The presence of this component was already suggested with the *BeppoSAX* observation (Grandi et al. 2006; Dadina 2007), indeed 3C 445 was detected with the PDS instrument. However, taking into account the large field of view (FOV) of this detector and the presence of a nearby (z=0.09) and bright cluster A2440 (located only 30' away) it was not possible to derive strong constraints on the amount of reflection. The presence of a strong reflection component was also suggested by the intensity of the Fe Kα line detected in the *BeppoSAX* and in the XMM-*Newton* observations (EW$\sim$ 120 eV Sambruna et al. 2007), which was consistent with being produced in reflection off a medium with high column density (Turner et al. 1997; Murphy & Yaqoob 2009).

Thanks to the smaller FOV of the HXD and more importantly to the *Swift*-BAT detection we can now confirm the presence of this component. In particular both the positional accuracy ($\sim$ 2') and offset with respect to 3C 445 ($\sim$ 0.5') reported 54-month Palermo-BAT catalog (Cusumano et al. 2010) are compatible with the emission from the center of 3C 445. As shown in Fig. 6, the averaged *Swift*-BAT spectrum is in agreement with the one obtained with *Suzaku*. This suggests that there is no strong variability of the intrinsic emission, but more importantly that contamination from the nearby cluster is unlikely to be present.

As shown in section 3.3, the amount of reflection measured is $R \sim 0.9$ implying a covering factor of the cold reflector of about 2π steradians. Furthermore, as we showed in the previous section the primary X-ray emission of 3C 445 is obscured by a high column density absorber ($N_H \sim 10^{23}\mathrm{cm}^{-2}$) with a covering factor of about 80%. In the hypothesis that the absorber is neutral the predicted extinction in the optical band would then far exceed the observed reddening of the source ($E_{B-V} \sim 1$ Crenshaw et al. 1988). In particular a scenario where our line of sight intercepts a homogeneous parsec scale torus is difficult to reconcile with the observational evidence, from the soft X-ray and optical band, that we are seeing the innermost region of this AGN. On the other hand the inclination angle from the jet ($\sim$ 60°) combined with the current estimates of the average opening angle of the "torus" implies that we might be looking at the nucleus of 3C 445 on the edge of this putative torus.

Though we note that data with a high-resolution calorimeter at the Fe Kα line energy are necessary to resolve the line complex LETG data (Reeves et al. 2010) and with the measured FWHM of the Hα ($\sim$ 6400 km s^{-1} Eracleous & Halpern 1994) and H β ($\sim$ 3000 km/s). The Fe Kα line could then be in part produced either in the outer part of the accretion disk or in the BLR. We note however that the relatively high EW of the Fe Kα line implies the presence of a Compton thick reflector, which is also confirmed by the detection of a strong reflection component. Indeed in order to be produced in transmission the observed EW of Fe Kα requires a higher column density absorber than the one measured with lower energy cutoff.

We thus tested the new model for the toroidal reprocessor[6] (Murphy & Yaqoob 2009), keeping the soft X-ray emitter modelled with a single ionised zone and we found that the intensity of the Fe Kα line and of the higher energy emission require the presence of a reprocessor with a column density $N_{\rm H} \sim 6.5 \times 10^{23}\mathrm{cm}^{-2}$ viewed at $\sim$ 60°, which is remarkably in agreement with the inclination of the system as derived from the radio observations (Eracleous & Halpern 1998). We note however that the photon index is now harder ($\Gamma \sim 1.5$) and there are some residuals in the 2–5 keV band suggesting the presence of a second absorber. We thus included a second and ionised absorber with no net outflowing velocity, qualitatively we note that we now have an excellent representation of the overall curvature of the X-ray emission. While the parameters of the ionised absorber are similar to the one derived with the REFLIONX model, we found that the reprocessor responsible for the Fe Kα line has a column density of $N_{\rm H} \sim 1.4 \times 10^{24}\mathrm{cm}^{-2}$ and as before it is viewed at $\sim$ 60°, the photon index is now $\Gamma \sim 1.8$. Qualitatively both these tests show us that a high column density mirror responsible for the Fe Kα line and the Compton reflection component is present and it could be associated with the part of the putative torus lying close to the plane of the accretion disk.

One possibility is that the photoionised emission line clouds, although located closer to the central SMBH, are lifted above the system's equatorial plane; our line of sight would then intercept the high column density absorber/reflector on a sub parsec scale but also have an unobscured view of BLR emission, where the optical and soft X-ray emission lines are produced. The alternative scenario which is suggested by the clumpy and neutral absorber, required to model the X-ray emission of 3C 445, is that the absorber/reflector is not a uniform "donut-like" structure and as proposed in recent models (Risaliti et al. 2002; Elitzur 2008; Maiolino et al. 2010) is clumpy and composed by many small and dense clouds, which could extend further in with respect to putative torus and are not simply obscuring the BLR but are part of the BLR themselves (Risaliti et al. 2009a,b). In this hypothesis our line of sight could then intercept a rather large number of clouds, which absorb/reflect the primary continuum but at the same time may also produce the the broad emission lines from innermost ionised clouds.

4.3 The nature of the X-ray absorber: a variable ionised absorber?

As shown in section 3.4, an alternative scenario to a clumpy and neutral absorber is an ionised absorber. This scenario naturally

accounts for the discrepancy between the optical and the X-ray band, indeed this mildly ionised absorber could be similar to the warm absorbers observed in the X-ray spectra of radio quiet AGN (Crenshaw et al. 2003; Blustin et al. 2005; McKernan et al. 2007; Turner & Miller 2009), which appear to be outflowing with velocity of 100-1000 km/s and could be associated with the presence of disk winds (King & Pounds 2003).

As discussed in a companion paper (Reeves et al. 2010) the presence of an ionised absorber, with the same ionisation level and column density, associated with a disk wind is strongly supported by the deep observation with high spectral resolution which provides more stringent constraints on the velocity of this absorber ($v_{\rm out} = 0.034 \pm 0.002c$) and on the launch radius ($R \sim 10^{16} - 10^{17}$cm). As also shown in that paper at this distance the likely density of the absorbing gas would be $\sim 10^{10}$ cm^{-3}, which would imply a $\Delta R \sim 10^{13}$ cm and a $\Delta R/R \sim 10^{-3}$ and thus suggesting a highly clumped absorber. It was also suggested that the clumpiness of this absorber would produce short-timescale variations of the observed column density, as seen in other Seyferts.

Indeed, the observed difference between the *Chandra* and *Suzaku* spectra could be explained with variability of this low ionisation absorber, not in terms of the covering factor or $N_{\rm H}$ of the absorber but in terms of its velocity. This is not surprising indeed not only red- and blueshifted absorption lines are predicted in several theoretical models of failed disk winds (Proga & Kallman 2004; Sim et al. 2010) or of aborted jet (Ghisellini et al. 2004) but also these models predict the outflows to be unstable and to show variability. In particular, outflows and jets could be produced intermittently and/or they could not have enough power to escape the system and eventually fall back into the accretion disk. This will affect the expected signatures that this warm gas imprints on the primary X-ray emission, which will produce transient absorption features and variability of the derived outflowing velocities and their EW as observed in several sources (Braito et al. 2007; Porquet et al. 2007; Dadina et al. 2005; Risaliti et al. 2005; Turner et al. 2008, 2010; Miller et al. 2010; Lobban et al. 2010).

An alternative scenario ascribes the difference between *Chandra* and *Suzaku* spectra to a further ionised and fast outflowing absorption component, detected only with the *Suzaku* observation and characterised by a high ionisation and column density ($N_{\rm H} \sim 10^{24}$cm^{-2}). In this scenario the properties of the low ionisation absorber are thus the same as the one derived with the *Chandra* observation (i.e., distance $R \sim 10^{16} - 10^{17}$cm and clumpiness $\Delta R/R \sim 10^{-3}$). For the high ionisation absorber, although in the *Suzaku* data the parameters of this absorber not well constrained, we can derive a order of magnitude estimate on its likely location from the values measured for the ionisation parameter ($\xi \sim 5$ erg cm s^{-1}), the outflow velocity ($v_{\rm out} \sim 0.04c$) and the column density. We can thus use the relation between these quantities and the illuminating continuum luminosity: $L_{\rm ion}/\xi = nR^2$, where $L_{\rm ion}$ is the intrinsic 1–1000 Rydberg luminosity (3×10^{44} erg s^{-1}), assuming the thickness of the clouds $\Delta R = N_H/n$ is less than the distance R, $\Delta R/R << 1$ we found $R < 5 \times 10^{15}$cm (or ~0.001 pc), which points towards an association of this absorbers with a wind launched off the disk at a sub-parsec distance from the central BH.

close to the central X-ray source. This could be associated with the presence of a disk wind which either is launched sporadically or it is highly clumped. However, in the absence of any stringent constraints on the launch radius we cannot speculate more as to whether these two absorbers are part of a single clumpy wind, where the lower ionisation component is associated to higher density clouds confined in the homogeneous highly ionised flow, or if the two components are part of single stratified medium. In order to determine whether it is a single and variable ionised absorber or a multi-phase wind would require higher resolution observations with instruments such as the calorimeter which will fly with Astro-H. These observations will allow to establish the complex nature and kinematics of this absorber confirming the presence of blueshifted absorption lines from highly ionised iron.

5 CONCLUSION

We have presented the results of a deep *Suzaku* observation of the BLRG 3C 445 which shows a complex absorbed X-ray spectrum. We confirm the results obtained with the previous XMM-*Newton* observation which unveiled the presence of several soft X-ray emission lines. The *Suzaku* and *Swift* spectra allowed us to measure a strong reflection component, which we associate with the presence of a high column density matter which is not in the line of sight. The primary X-ray continuum is strongly absorbed either by a partially covering neutral or a mildly ionised absorber, which could be associated with an accretion disk wind.

Regarding the overall geometry of 3C 445, we know from the radio observations that we are seeing the central regions of this AGN at a relatively large inclination. A plausible scenario is that we are viewing along the edge of the putative torus through either a partially covering neutral absorber or mildly ionised absorber, which could be associated with an equatorial disk-wind. In both the scenarios with an ionised or neutral absorber, the matter needs to be clumped, such as that the observer has a direct view of the clouds responsible of the soft X-ray and optical lines, which could be in part uplifted with respect to the equatorial plane. A possible schematic diagram for the geometry of the inner regions of 3C 445 is presented in Figure 8 of Reeves et al. 2010, a new addition to that schematic view is that *Suzaku* provided evidence for the presence also of a Compton-thick reflector. We find no evidence that our line of sight intercepts this Compton-thick absorber which is responsible for the reflected component and Fe Kα line. This absorber could be either associated with denser clouds probably located in the equatorial plane of the torus or of the clumpy absorber or the outer part of the disk-wind.

ACKNOWLEDGMENTS

This research has made use of data obtained from the Suzaku satellite and data obtained from the High Energy Astrophysics Science Archive Research Center (HEASARC), provided by NASA's Goddard Space Flight Center. VB acknowledge support from the UK STFC research council.

Ballantyne, D. R., Fabian, A. C., & Ross, R. R. 2002, MNRAS, 329, L67
Ballantyne, D. R. 2007, Modern Physics Letters A, 22, 2397
Baumgartner et al. 2010 ApJS submitted
Bianchi, S., Guainazzi, M., & Chiaberge, M. 2006, A&A, 448, 499
Boldt, E. 1987, Phys. Rep., 146, 215
Braito, V., et al. 2007, ApJ, 670, 978
Brinkman, A. C., et al. 2000, ApJ, 530, L111
Blustin, A. J., Page, M. J., Fuerst, S. V., Branduardi-Raymont, G., & Ashton, C. E. 2005, A&A, 431, 111
Cattaneo, A., et al. 2009, Nature, 460, 213
Corbett, E. A., Robinson, A., Axon, D. J., Young, S., & Hough, J. H. 1998, MNRAS, 296, 721
Crenshaw, D. M., Peterson, B. M., & Wagner, R. M. 1988, AJ, 96, 1208
Crenshaw, D. M., Kraemer, S. B., & George, I. M. 2003, ARA&A, 41, 117
Cusumano, G., et al. 2010, A&A, 510, A48
Dadina, M., Cappi, M., Malaguti, G., Ponti, G., & de Rosa, A. 2005, A&A, 442, 461
Dadina, M. 2007, A&A, 461, 1209
Dickey, J. M., & Lockman, F. J. 1990, ARA&A, 28, 215
Eracleous, M., & Halpern, J. P. 1998, ApJ, 505, 577
Eracleous, M., & Halpern, J. P. 1994, ApJS, 90, 1
Elvis, M. 2006, Mem. Soc. Astron. Italiana, 77, 573
Elitzur, M. 2008, New A Rev., 52, 274
Evans, I. N., et al. 2010, ApJS, 189, 37
Fabian, A. C. 2010, IAU Symposium, 267, 341
Fabian, A. C., Rees, M. J., Stella, L., & White, N. E. 1989, MNRAS, 238, 729
Grandi, P., Foschini, L., Masetti, N., & Palazzi, E. 2004, A&A, 418, 907
Grandi, P., Malaguti, G., & Fiocchi, M. 2006, ApJ, 642, 113
Grandi, P., Guainazzi, M., Cappi, M., & Ponti, G. 2007, MNRAS, 381, L21
Gruber, D. E., Matteson, J. L., Peterson, L. E., & Jung, G. V. 1999, ApJ, 520, 124
Ghisellini, G., Haardt, F., & Matt, G. 2004, A&A, 413, 535
Guainazzi, M., & Bianchi, S. 2007, MNRAS, 374, 1290
King, A. R., & Pounds, K. A. 2003, MNRAS, 345, 657
Kallman, T. R., Palmeri, P., Bautista, M. A., Mendoza, C., & Krolik, J. H. 2004, ApJS, 155, 675
Kinkhabwala, A., et al. 2002, ApJ, 575, 732
Koyama, K., et al. 2007, PASJ, 59, 23
Kokubun, M., et al. 2007, PASJ, 59, 53
Kronberg, P. P., Wielebinski, R., & Graham, D. A. 1986, A&A, 169, 63
Liedahl, D. A. 1999, LNP Vol. 520: X-Ray Spectroscopy in Astrophysics, 520, 189
Liedahl, D. A., & Paerels, F. 1996, ApJ, 468, L33
Leahy, J. P., Black, A. R. S., Dennett-Thorpe, J., Hardcastle, M. J., Komissarov, S., Perley, R. A., Riley, J. M., & Scheuer, P. A. G. 1997, MNRAS, 291, 20
Longinotti, A. L., Nucita, A., Santos-Lleo, M., & Guainazzi, M. 2008, A&A, 484, 311
Longinotti, A. L., et al. 2010, A&A, 510, A92
Magdziarz, P., & Zdziarski, A. A. 1995, MNRAS, 273, 837
McKernan, B., Yaqoob, T., & Reynolds, C. S. 2007, MNRAS, 379, 1359
Miller, L., Turner, T. J., Reeves, J. N., Lobban, A., Kraemer, S. B., & Crenshaw, D. M. 2010, MNRAS, 403, 196
Mitsuda, K., et al. 2007, PASJ, 59, 1
Murphy, E. M., Lockman, F. J., Laor, A., & Elvis, M. 1996, ApJS, 105, 369
Murphy, K. D., & Yaqoob, T. 2009, MNRAS, 397, 1549
Narayan, R., & Yi, I. 1995, ApJ, 444, 231
Ogle, P. M., Mason, K. O., Page, M. J., Salvi, N. J., Cordova, F. A., McHardy, I. M., & Priedhorsky, W. C. 2004, ApJ, 606, 151
Porquet, D., et al. 2007, A&A, 473, 67
Proga, D., & Kallman, T. R. 2004, ApJ, 616, 688
Ptak, A., & Griffiths, R. 2003, Astronomical Data Analysis Software and Systems XII, 295, 465
Reeves, J. N., Sambruna, R. M., Braito, V., & Eracleous, M. 2009, ApJ, 702, L187
Reeves, J. N., Gofford, J., Braito, V., & Sambruna, R. 2010, ApJ, 725, 8
Reeves, J. N., & Turner, M. J. L. 2000, MNRAS, 316, 234
Risaliti, G., Elvis, M., & Nicastro, F. 2002, ApJ, 571, 234
Risaliti, G., Bianchi, S., Matt, G., Baldi, A., Elvis, M., Fabbiano, G., & Zezas, A. 2005, ApJ, 630, L129
Risaliti, G., et al. 2009, MNRAS, 393, L1
Risaliti, G., et al. 2009, ApJ, 696, 160
Ross, R. R., Fabian, A. C., & Young, A. J. 1999, MNRAS, 306, 461
Ross, R. R., & Fabian, A. C. 2005, MNRAS, 358, 211
Rudy, R. J., & Tokunaga, A. T. 1982, ApJ, 256, L1
Sambruna, R. M., et al. 2009, ApJ, 700, 1473
Sambruna, R. M., George, I. M., Mushotzky, R. F., Nandra, K., & Turner, T. J. 1998, ApJ, 495, 749
Sambruna, R. M., Eracleous, M., & Mushotzky, R. F. 1999, ApJ, 526, 60
Sambruna, R. M., Eracleous, M., & Mushotzky, R. F. 2002, New Astronomy Review, 46, 215
Sambruna, R. M., Reeves, J. N., & Braito, V. 2007, ApJ, 665, 1030
Sim, S. A., Proga, D., Miller, L., Long, K. S., & Turner, T. J. 2010, MNRAS, 408, 1396
Spergel, D. N., et al. 2003, ApJS, 148, 175
Steenbrugge, K. C., et al. 2005, A&A, 434, 569
Takahashi, T., et al. 2007, PASJ, 59, 35
Tombesi, F., Sambruna, R. M., Reeves, J. N., Braito, V., Ballo, L., Gofford, J., Cappi, M., & Mushotzky, R. F. 2010, ApJ, 719, 700
Torresi, E., Grandi, P., Guainazzi, M., Palumbo, G. G. C., Ponti, G., & Bianchi, S. 2009, A&A, 498, 61
Torresi, E., Grandi, P., Longinotti, A. L., Guainazzi, M., Palumbo, G. G. C., Tombesi, F., & Nucita, A. 2010, MNRAS, 401, L10
Tueller, J., et al. 2010, ApJS, 186, 378
Turner, T. J., George, I. M., Nandra, K., & Mushotzky, R. F. 1997, ApJ, 488, 164
Turner, T. J., Kraemer, S. B., George, I. M., Reeves, J. N., & Bottorff, M. C. 2005, ApJ, 618, 155
Turner, T. J., Reeves, J. N., Kraemer, S. B., & Miller, L. 2008, A&A, 483, 161
Turner, T. J., & Miller, L. 2009, A&A Rev., 17, 47
Turner, T. J., Miller, L., Reeves, J. N., Lobban, A., Braito, V., Kraemer, S. B., & Crenshaw, D. M. 2010, ApJ, 712, 209